Articles
doi.org/10.1002/batt.201900170

Chemistry Europe
European Chemical Societies Publishing

Approaching Reactive $KFePO_4$ Phase for Potassium Storage by Adopting an Advanced Design Strategy

Irin Sultana,[a, b] M. Mokhlesur Rahman,*[b] Srikanth Mateti,[b] Neeraj Sharma,[c] Shaoming Huang,*[a] and Ying Chen*[b]

Pristine $KFePO_4$ is electrochemically inactive towards potassium, which suggests that K^+ ion migration is unfavorable in the $KFePO_4$ structure. Therefore, it is a challenge to create a reactive structure of $KFePO_4$ towards reversible potassium insertion/extraction. In this study, we have fabricated reactive $KFePO_4$ phase by adopting high-energy ball milling technique where tiny nanoparticles (~1.0-1.5 nm) of $KFePO_4$ are created and embedded in the Super P carbon black matrix, which provides conductivity and helps to stabilize the electrode structure. The combination of nano-sizing and the conductive matrix appears to activate electrochemical reactivity. The obtained carbon incorporated $KFePO_4$ material appears to be amorphous. The electrode produces an average operational potential of ~2.5 V (vs K^+/K) with high capacity retention of 90 mAh g^{-1}. It is anticipated that this work could pave the way for further studies on cathodes and generate huge attention to the role of ball milling and particle size control on electrochemical activity of $KFePO_4$ materials for the development of PIBs.

1. Introduction

Potassium-ion batteries (PIBs) are electrochemical energy storage cells with many advantages. Both theoretical calculations and experimental observations reveal that the K^+/K couple exhibits the lowest redox potential among lithium and sodium couples in some non-aqueous electrolytes,[1,2] suggesting that potassium-ion (K-ion) high voltage batteries with high energy density are possible.[3] Like sodium, potassium also does not alloy with aluminum at low potentials, which eliminates expensive copper current collectors at anode, which is an essential requirement for lithium-ion batteries.[4] However, a key obstacle for the practical realization of this emerging technology is the lack of suitable electrode materials that are capable to reversibly intercalate or insert K^+ with high capacity, suitable voltage, fast kinetics, and reliable cycle life. This is predominantly related to the larger size K^+ ($Li^+ < Na^+ < K^+$, 0.76 Å < 1.02 Å < 1.38 Å) which can cause damage or a greater change in the electrode host structures upon cycling.[5–7] To explore materials, we took some initiatives and developed a series of new alloy anodes based on tin, antimony, and phosphorous for PIBs.[8–11] These early results have stimulated research community significantly. To further advance the field, we have paid attention on cathode materials for the development of PIBs.

To date, four categories of cathode materials have been extensively explored which are layered oxides, Prussian blue analogues (PBAs), polyanionic compounds, and organic compounds. These have been evaluated for non-aqueous PIBs since 2004.[7] Polyanionic compounds are considered promising cathode materials due to their high stability against oxygen loss and the ability to tune the redox voltage through the inductive effect, however, no research progress is realized with the polyanionic based $KFePO_4$ compound. In 2014, Mathew et al.[12] prepared amorphous $FePO_4$ and evaluated this as a PIB cathode for the first time. Even though the amorphous $FePO_4$ delivered initial discharge capacity of 156 mAh g^{-1} at 5 mA g^{-1}, it is not suitable as PIB cathode because a pre-potassiation step is necessary either by chemical or electrochemical methods to insert potassium into the structure.

In 2018, Komoba et al.[13] investigated the electrochemical potassiation into delithiated triphylite, $FePO_4$, prepared by electrochemical delithiation of $LiFePO_4$. Unfortunately, the crystal structure of $FePO_4$ was not suitable to accommodate large size of K^+, leading to a non-reversible charge/discharge process. Komoba et al.[14] further attempted to improve this material and synthesized carbon incorporated variants or $KFePO_4$/C. While $KFePO_4$/C was successfully prepared, the material was electrochemically nonreactive towards potassium, which may be due to its relative crystalline state combined with micrometer size particles. As a result, unsatisfactory electrochemical performance and a low reversible capacity of 25 mAh g^{-1} at 7.1 mA g^{-1} current was achieved.

In a typical rechargeable battery, the choice of ion-insertion cathodes, either crystalline or amorphous, greatly contributes to the storage/specific capacity.[12] The storage capacities delivered by crystalline hosts are critically dependent on

[a] Dr. I. Sultana, Prof. S. Huang
School of Materials and Energy,
Guangdong University of Technology,
Guangzhou 51006, Guandong, P.R. China
E-mail: smhuang@gdut.edu.cn
[b] Dr. I. Sultana, Dr. M. M. Rahman, Dr. S. Mateti, Prof. Y. Chen
Institute for Frontier Materials, Deakin University,
Geelong Waurn Ponds, VIC 3216 (Australia)
E-mail: m.rahman@deakin.edu.au
ian.chen@deakin.edu.au
[c] Dr. N. Sharma
School of Chemistry, University of New South Wales,
Sydney, New South Wales 2052, Australia

Supporting information for this article is available on the WWW under https://doi.org/10.1002/batt.201900170

various factors such as crystal orientation and structural stability, formation of active facets, ion migration path, phase transitions, and the crystal imperfections/defects.[12] Moreover, limited ion movement at the phase-transition interface can eventually lower the storage capacities in crystalline hosts.[12,15] In contrast, amorphous electrodes possess a number of potential benefits including short-range structural ordering, improved kinetics, high surface area, no macroscopic phase transitions, and the ability to accommodate potentially more distortions relative crystalline electrodes, which can lead to better specific capacities and a more stable cycle life.[16–18] Thereby, such amorphous materials may prove to be an ideal opportunity to reversibly store K^+.

To utilize the advantages of amorphous over crystalline electrodes, we prepare and report amorphous $KFePO_4$/C electrodes (denoted as AM-$KFePO_4$/C) for PIBs. It is demonstrated that high-energy ball milling with an external magnet positioned at a 45° angle is exceptionally suitable method for amorphizing crystalline $KFePO_4$. Furthermore, the particle size is simultaneously reduced to extremely nanometer level (~1.0–1.5 nm) and homogeneously distributed and embedded into the Super P Li carbon matrix during ball-milling. The result is an amorphous composite microstructure. The obtained amorphous $KFePO_4$/C electrode can function as an effective cathode material for PIBs in a wide range of potential windows. When used as cathodes within 1.5–3.5 V a reversible capacity of 47 mAh g^{-1} was achieved and within 1.5–4.1 V a reversible capacity of 90 mAh g^{-1} was achieved at 10 mA g^{-1} current density. Hence, preparation of materials, crystal structure and the prospects of electrochemical performance of this cathode are reflected in this paper.

2. Results and Discussion

XRD data were collected to study the crystal structure and phase purity of pristine $KFePO_4$ and composite $KFePO_4$/C samples (Figure 1a). The diffraction peaks for the crystalline pristine $KFePO_4$ could be indexed to the monoclinic phase of $KFePO_4$ [ICSD No. 415458]. Figure 1b shows a Rietveld refined fit of the $KFePO_4$ model to the XRD data. Particle size broadening from the XRD data is ~120 nm for the pristine $KFePO_4$ and the refined structural parameters of the $KFePO_4$ are summarized in Table S1. The XRD pattern of the composite $KFePO_4$/C is visibly different compared to the XRD pattern of the pristine $KFePO_4$. No strong diffraction peaks are visible in $KFePO_4$/C, suggesting that the sample is predominantly amorphous or extremely nanosized.

In order to verify textural properties of the pristine $KFePO_4$ and ball milled AM-$KFePO_4$/C samples, nitrogen adsorption/desorption isotherms, corresponding pore size distributions and pore volume were measured and determined (Figure 2). Even though the shape of the isotherm curves in Figure 2 a, c can be classified as type IV with an H1 hysteresis loop at a relative pressure (P/P_0) ~0.8–1.0,[19,20] however, materials may not be considered as mesoporous because of low surface area. The obtained high BET surface area (~7 $m^2 g^{-1}$) of the ball

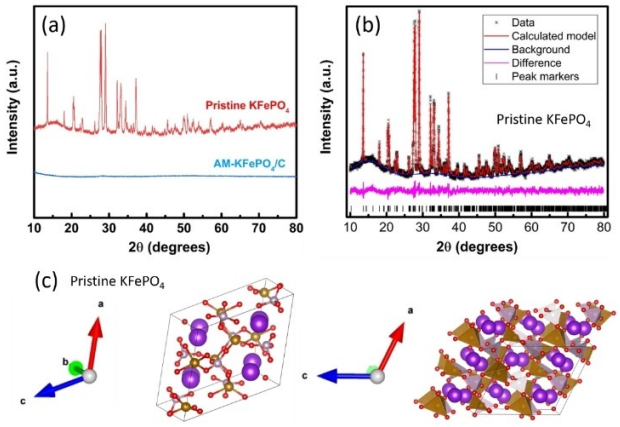

Figure 1. a) XRD patterns of the samples. b) Rietveld-refined fit of the $KFePO_4$ structural model to the XRD data for pristine $KFePO_4$. c) Crystal structure of the pristine $KFePO_4$ with oxygen shown in red, potassium in purple and iron in brown and phosphorus in light purple, ball and stick on the left and polyhedral on the right.

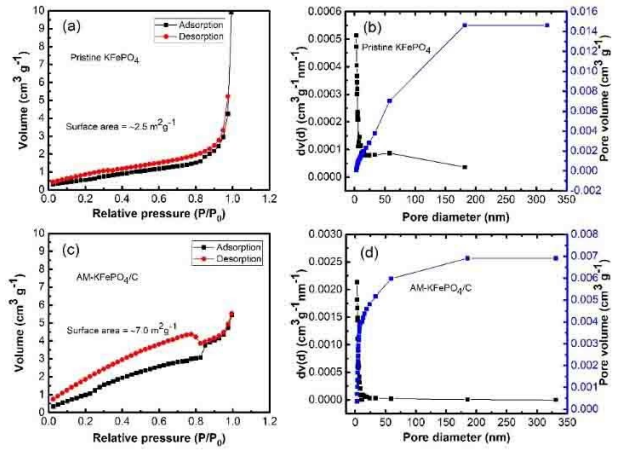

Figure 2. Nitrogen adsorption-desorption isotherms and corresponding pore-size and pore volume distributions as analyzed by Barrette-Joynere-Halenda (BJH) method: a, b) pristine $KFePO_4$. c, d) amorphous $KFePO_4$/C (AM-$KFePO_4$/C).

milled AM-$KFePO_4$/C sample (compared to pristine $KFePO_4$ sample ~2.5 $m^2 g^{-1}$) could be ascribed to the crystal defects and particle size reduction due to milling. The corresponding pore size distributions and pore volume curves are also shown in Figure 2b, d. The BET test results including specific surface area, pore size, and pore volume of the samples are shown in Table S2. The results are in good agreement with microscopy observations as depicted in Figure 3. During ball milling, $KFePO_4$ particles and Super P Li carbon black were mechanical milled by magneto-ball mill, which reduces particle size and increases the total surface area. The relatively large specific surface offers a large contact area between the electrolyte and the electrode materials, and promotes ion diffusion from the electrolyte to the active sites with less resistance and reduces diffusion distances for ions during their insertion into or reaction with the structure.[21,22] Hence, it is anticipated that the

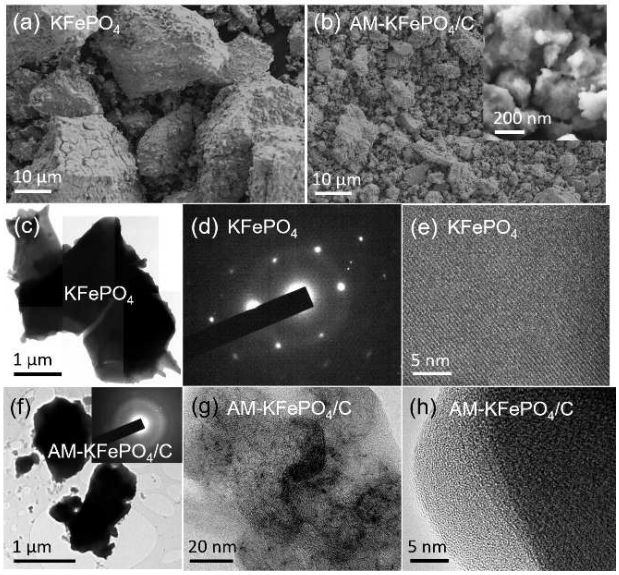

Figure 3. Electron microscopy investigations: SEM images of a) pristine $KFePO_4$. b) AM-$KFePO_4$/C; TEM investigation (c-h): c) a bright-field image. d) SAED pattern. e) lattice fringes of pristine $KFePO_4$; f) a bright-field image with inset SAED pattern. g) high-resolution bright-field image, and h) HRTEM image (shows no lattice fringes) of AM-$KFePO_4$/C.

ball-milled AM-$KFePO_4$/C may deliver a high reversible capacity when compared to the pristine $KFePO_4$.

To reveal the microscopic structure of the materials, scanning electron microscopy (SEM) and transmission electron microscopy (TEM) studies were carried out (Figure 3). The typical morphology of pristine $KFePO_4$ is depicted in Figure 3a. The low magnification SEM image shows that $KFePO_4$ consists of micrometer-sized large clusters with the size in the range of 5–50 μm. Figure 3b demonstrates low magnification SEM image of the ball milled AM-$KFePO_4$/C sample. A significant change in the morphology is observed between pristine $KFePO_4$ and AM-$KFePO_4$/C samples. The ball mill step significantly reduces the micrometer-sized large clusters of $KFePO_4$. High magnification SEM image shows that the AM-$KFePO_4$/C sample is composed of agglomerated small clusters of tiny nanoparticles (inset, Figure 3b). Figure 3c-e shows TEM analysis of the pristine $KFePO_4$ which consists of large particles as shown in a bright-field image in Figure 3c. A number of bright diffraction spots in the corresponding SAED pattern (Figure 3d) as well as lattice fringes (Figure 3e) indicate that pristine $KFePO_4$ is crystalline as expected from the XRD analysis. TEM analysis of AM-$KFePO_4$/C sample is presented in Figure 3f-h. Figure 3f shows a bright field image and a corresponding SAED pattern (inset). It is obvious that sample consists of small clusters composed of nano particles. However, the SAED pattern consists of few tiny bright spots along with diffuse rings, indicating sample is extremely nano or nearly amorphous in nature. High-resolution TEM (HRTEM) image shows that no distinguishable lattice fringes observed, indicating predominant amorphous nature of the ball milled $KFePO_4$/C sample (Figure 3h). This result is well supported by XRD analysis as depicted in Figure 1a. HRTEM image also confirms that the ball mill step reduces particle size and produces tiny nanoparticles (~1.0–1.5 nm) of $KFePO_4$ that are embedded into Super P carbon black matrix (can be seen as tiny black dots) as presented in Figure 3g. To support TEM analysis, SEM-EDS investigations were carried out (Figure S1). EDS mapping shows the bright spots which correspond to the presence of the elements of K, Fe, P, O, and C, respectively. The results show that carbon particles are distributed uniformly throughout the whole area of $KFePO_4$ nanoparticles. A high-angle annular dark-field (HAADF) STEM image of the AM-$KFePO_4$/C sample further confirmed that sample consists of super P Li carbon black (light grey color) decorated with quite homogeneously distributed nanoscale particles of $KFePO_4$ (bright contrast in the image) (Figure S2).Such homogeneous dispersion and intimate connectivity between $KFePO_4$ nanoparticles and super p carbon black can be expected to significantly increase the conductivity.

The potassium storage performance of the electrodes was evaluated in coin-type half-cells (CR 2032) using potassium as the counter and reference electrode. Figure 4a compares cycling performance of the electrodes in the potential range of 3.5–1.5 V vs. K^+/K. The ball milled AM-$KFePO_4$/C electrode shows a reversible capacity of 47 mAh g^{-1} with a good retention of ~84% (with respect to the first reversible capacity of 54 mAh g^{-1}) at 10 mA g^{-1} after 50 cycles. In contrast, pristine $KFePO_4$ electrode shows negligible capacity of 10 mAh g^{-1} at 10 mA g^{-1} after 50 cycles within the same potential rage of 3.5–1.5 V vs. K^+/K. At the first cycle, the AM-$KFePO_4$/C electrode exhibits charge/discharge capacities of 55/53 mAh g^{-1} (Figure 4c), corresponding to the initial Coulombic efficiency of 97% (Figure 4d). Additionally, the charge and discharge curves (except first cycle) of the subsequent 2–50 cycles are very similar, indicating stable potassium extraction/insertion process within the AM-$KFePO_4$/C electrode. In the case of pristine $KFePO_4$ electrode, potential hysteresis and low charge/discharge capacities of 25/22 mAh g^{-1} (Figure 4b) with a Coulom-

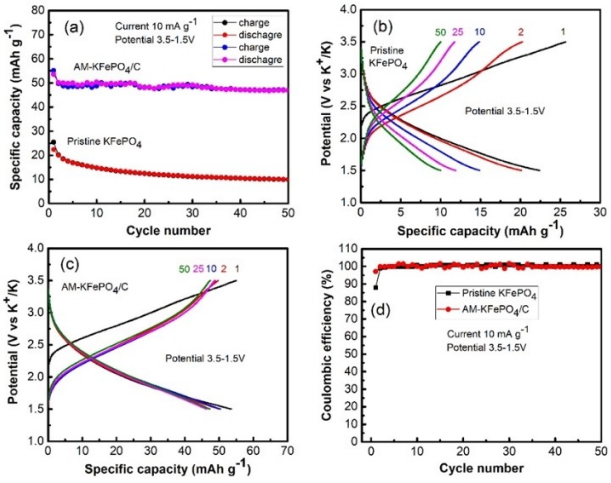

Figure 4. Electrochemical performance of pristine $KFePO_4$ and AM-$KFePO_4$/C electrodes within the potential range of 3.5–1.5 V at a current density of 10 mA g^{-1}: a) Cycling performance up to 50 cycles; b, c) corresponding galvanostatic charge/discharge potential profiles for the selected cycles of 1st, 2nd, 25th and 50th; d) corresponding Coulombic efficiencies.

bic efficiency of 88% (Figure 4d) are realized. However, charge/discharge profiles of the AM-$KFePO_4$/C electrode are different from the cycles of crystalline $NaFePO_4$ or $LiFePO_4$ materials, whose have typical potential plateau.[23,24] Smooth slopes are observed with the evolution of potassium-ion extraction/insertion in the AM-$KFePO_4$/C electrode, which is typical for amorphous metal phosphate based electrodes.[25]

The electrochemical performance of the AM-$KFePO_4$/C electrodes was further examined within an extended potential range of 4.1–1.5 V (Figure 5). Interestingly, the AM-$KFePO_4$/C electrode is capable to operate smoothly at the charge cut-off potential of 4.1 V with a reversible capacity of 90 mAh g^{-1} (90% reversible capacity retention) at 10 mA g^{-1} current after 50 cycles (Figure 5a). The corresponding charge-discharge potential profile of the AM-$KFePO_4$/C electrode is presented in Figure 5b. First cycle charge/discharge capacities of 105/99 mAh g^{-1} with an initial Coulombic efficiency of 94% was achieved (Figure 5b, c). After the first cycle, Coulombic efficiency reached close to ~100% in the subsequent cycles, indicating high reversibility of the electrode. Upon charging the cell (Figure 5b), the potential exhibits a gradual increase from the open circuit potential to 4.1 V. Upon discharge (Figure 5b), a pronounced drop in potential is observed in the beginning. At 3.0 V, the slope changes with a pseudo-plateau to 1.8 V, followed by a slow decrease to the cut-off potential of 1.5 V.

The potential features observed in the charge/discharge curves are consistent with the CV results obtained at a scan rate of 0.5 mV s^{-1} in the potential range of 4.1–1.5 V (Figure 6). A broad anodic peak located ~2.8 V corresponds to the charge process, in which K^+ ions are extracted from $KFePO_4$. The broad cathodic peak located at around 1.8 V corresponds to the discharge process, in which K^+ ions are inserted to the $KFePO_4$. Such a broad redox peaks is consistent with the smooth slopes in the charge/discharge curves and may indicate a continuous single-phase depotassiation/potassiation reaction,[26] confirming amorphous nature of the electrodes.[25] The CV curves of the AM-$KFePO_4$/C electrode remained almost unchanged in subsequent cycles, demonstrating high reversibility and stable electrochemical reaction.

Electrochemical impedance spectroscopy (EIS) measurements were carried out for the fresh cells (open circuit potential

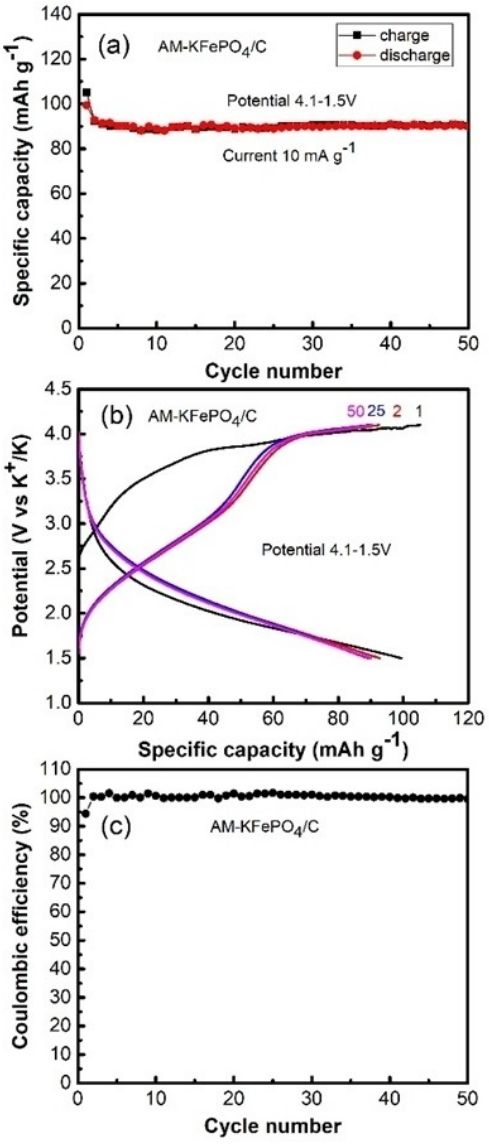

Figure 5. Electrochemical performance of the AM-$KFePO_4$/C electrodes within an extended potential range of 4.1–1.5 V at a current density of 10 mA g^{-1}: a) cycling performance up to 50 cycles; b) corresponding galvanostatic charge/discharge potential profiles for the selected cycles of 1st, 2nd, 25th and 50th; c) corresponding Coulombic efficiencies.

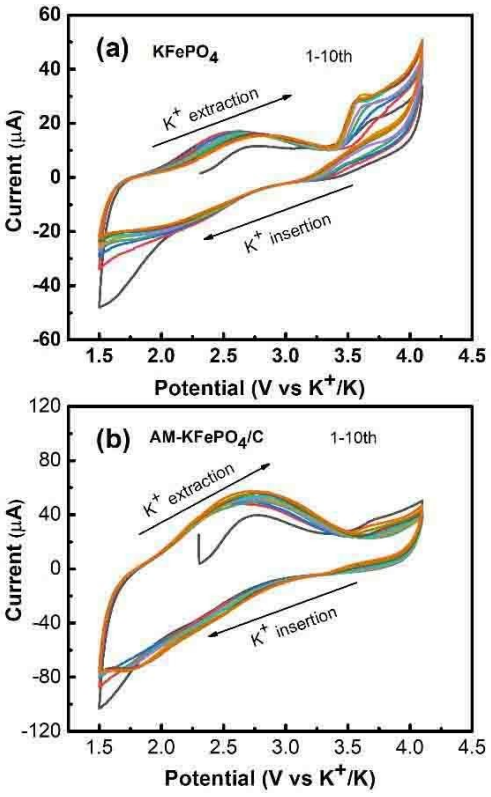

Figure 6. Cyclic voltammograms of the electrodes obtained up to 10 cycles at a scan rate of 0.5 mV s^{-1} in the potential range of 4.1–1.5 V: a) pristine $KFePO_4$. b) AM-$KFePO_4$/C electrodes.

(OCP) state) to gain insight into the improved electrochemical performance of the AM-$KFePO_4$/C electrode. Typical Nyquist plots recorded for both electrodes are presented in Figure 7 with an equivalent circuit, inset. In this equivalent circuit, R_s and R_{ct} are the ohmic resistance (total resistance of the electrolyte, separator, and electrical contacts) and the charge transfer resistance, respectively. CPE is the constant phase-angle element, involving double layer capacitance, and *W* represents the Warburg impedance, which is associated with the inclined line at low frequencies. Both plots display one compressed semicircle in the high to medium frequency region and a sloped line in the low frequency region. The diameter of each semicircle is related to the charge transfer resistance (R_{ct}), the smaller the diameter, the smaller the charge transfer resistance, and the higher the electronic conductivity.[27,28] Charge transfer resistance (R_{ct}) values are mainly focused on this measurement. The charge transfer resistance (R_{ct}) was calculated to be 8310 Ω for pristine $KFePO_4$ electrode, whereas it is 386 Ω for AM-$KFePO_4$/C electrodes. Such a smaller charge transfer resistance (R_{ct}) of the AM-$KFePO_4$/C sample indicates that AM-$KFePO_4$/C electrode has much easier charge transfer at the electrode-electrolyte interface and, consequently, a decreased overall internal cell resistance compared to the pristine $KFePO_4$ electrode. The incorporation of Super P Li carbon black into $KFePO_4$ materials and subsequent downsizing and amorphization and dispersion of $KFePO_4$ nanoparticles into the carbon matrix by the ball-milling process significantly enhances the conductivity of the AM-$KFePO_4$/C materials. The Super P Li carbon black provides conductive paths in the vicinity of the nanoparticles of $KFePO_4$ and is considered a key factor in the cycling stability improvements due to more efficient electronic and ion transport in the electrodes.

Non-reactive electrochemical nature of the pristine $KFePO_4$ electrode with potassium implies that morphological and structural features play a critical role for the improvement in the electrochemical performance of the AM-$KFePO_4$/C electrode. In this regard, several reasons could be responsible.[25] First, high-energy ball mill reduced particle size down to extremely nanometer level, which predominantly amorphous. Further, the milling simultaneously mixed and embedded nano particles of $KFePO_4$ into Super P Li carbon black matrix, and creates a composite microstructure. As a result, such electrode architecture is likely to feature a short diffusion distance for K^+, which promotes fast and reversible potassium ion insertion/extraction. Second, the ball milled AM-$KFePO_4$/C sample exhibits higher specific surface area of ~7 $m^2 g^{-1}$ as compared to that of the pristine $KFePO_4$ (~ 2.5 $m^2 g^{-1}$) sample. Such a relatively large specific surface area of the AM-$KFePO_4$/C sample is likely to result in an increased number of easily accessed insertion sites as well as simplifying the infiltration of the electrolyte into the bulk of the material/electrode that allows fast diffusion pathways for K^+ in liquid and solid phases with less resistance. At the same time, a longer electrochemical reaction can be maintained in the interface that drastically decreases the electrochemical polarization and improves the capacity utilization. Third, the amorphous nature of the AM-$KFePO_4$/C sample is likely to avoid lattice stress, which may allow freedom for a change in dimensions during K^+ insertion/extraction, leading to improved reversible capacity. However, it is important to note that potassium containing amorphous $KFePO_4$/C cathode can be a great advantage in the fabrication of prototype PIB with recently discovered high performance anode materials (such as graphite, P, Sn, and Sb) which would require K containing cathode materials.

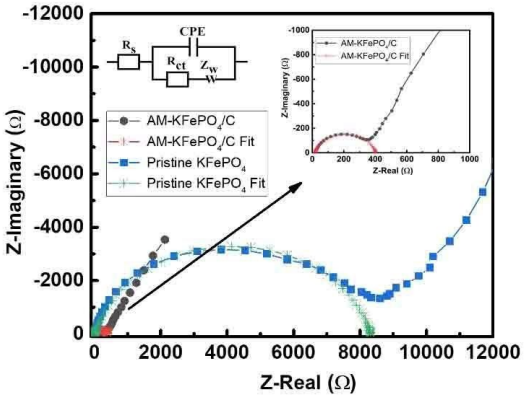

Figure 7. Electrochemical impedance spectra and the corresponding equivalent circuit (inset) model of the electrodes with fresh cells (without cycling).

3. Conclusions

Typically, pristine $KFePO_4$ structure is unfavorable for reversible K^+ storage. To create a reactive structure, an amorphization/particle reduction strategy is executed where crystal structure of the pristine $KFePO_4$ is abolished by adopting high-energy ball milling technique. During milling, tiny particles of $KFePO_4$ are created and simultaneously embedded into a Super P carbon matrix, forming potassium-containing amorphous nano composite cathode of $KFePO_4$/C. The obtained electrochemical data demonstrates that the amorphous $KFePO_4$/C is capable to store potassium with a capacity retention of 90 mAh g^{-1} at 10 mA g^{-1} after 50 cycles. Moreover, the amorphous $KFePO_4$/C cathode promises huge potential to be coupled with K-free anodes rather than coupled with metallic K anode, which poses a potential safety risk. Therefore, this study opens new possibilities for the development of polyanionic based $KFePO_4$ cathode for future PIBs.

Experimental Section

Preparation of pristine $KFePO_4$

A two-step process was used to prepare the pristine $KFePO_4$ powder. Firstly, K_2CO_3 (Sigma-Aldrich, 99.99%), $FeC_2O_4 \cdot 2H_2O$ (Sigma-Aldrich, 99.99%), and $NH_4H_2PO_4$ (Sigma-Aldrich, 99.999%) with a molar ratio of 0.5:1:1 were loaded inside a stainless steel milling container together with four hardened steel balls (diameter of 25.4 mm). To achieve a homogeneous mixture, the powder was milled in a vertical rotating ball mill at a rotation speed of 160 rpm for 45 hr at room temperature under an argon atmosphere of 150 kPa. Secondly, the mixture was then calcined in a tube furnace under an argon (Ar) atmosphere at 350 °C for 5 hr, followed by a regrind and re-calcine under Ar at 800 °C for 10 hr.

Preparation of amorphous $KFePO_4$/C composite

To prepare amorphous $KFePO_4$/C composite, 2 gm of pristine $KFePO_4$ powder and 0.5 gm of Super P Li carbon black in a weight ratio of 4:1 were ball milled together with four hardened steel balls (diameter of 25.4 mm). A vertical rotating ball mill with a magnet position at 45° angle was used for this purpose. The powder was milled at a rotation speed of 160 rpm for 70 hr at room temperature under an argon atmosphere of 100 kPa. This composite is denoted as amorphous $KFePO_4$/C (AM-$KFePO_4$/C).

Materials characterization

X-ray diffraction (XRD) data were collected from samples on a PANalytical X'Pert Pro instrument using a Cu Kα radiation source ($\lambda = 1.54181$ Å) and operated at 40 KV with a 50 mA current. The Brunauer-Emmett-Teller (BET) surface area was measured using a Tristar 3000 micrometrics gas adsorption analyzer. Morphologies were examined using scanning electron microscopy (SEM, Carl Zeiss Supra 55 VP). Transmission electron microscopy (TEM) analysis was performed on a JEOL JEM 2100 operated at 200 kV. A high-angle annular dark-field (HAADF) image was obtained in a scanned TEM (STEM) mode.

Electrochemical characterization

To prepare battery electrodes, the pristine $KFePO_4$ powder was mixed with Super P Li carbon black and a binder, PVDF, in a weight ratio of 70:20:10 in a solvent (NMP). On the other hand, no further Super P Li carbon black was added for the preparation of battery electrodes with composite $KFePO_4$/C samples. The composite $KFePO_4$/C samples were mixed with a binder, PVDF, in a weight ratio of 90:10 in a solvent (NMP). The slurry was spread onto Al foil substrates with an average active material loading of 1.1–1.3 mg and these coated electrodes were dried in a vacuum oven at 100 °C for 24 h. The electrode was then pressed using a disc with a diameter of 25 mm to enhance the contact between the Al foil and active materials. Subsequently, the electrodes were cut to 1× 1 cm^2. CR 2032 coin-type half-cells were assembled in an Ar-filled glove box (Innovative Technology, USA). Potassium (K) metal was used as the counter/reference electrode and Whatman GF/F microfiber glass membranes were used as separators. The electrolyte was 0.75 M KPF_6 in a mixture of ethylene carbonate (EC) and diethyl carbonate (DEC) with a volume ratio of 1:1. The cells were galvanostatically charged/discharged at a current rate of 10 mA g^{-1} within potential ranges of 3.5–1.5 and 4.1–1.5 V vs K/K^+ using a computer controlled LAND battery system (Wuhan LAND, China). The cycling was performed in a thermostat box programmed to maintain a constant temperature of 25 °C during the tests. Cyclic voltammograms (CV) were recorded using an Ivium-n-state electrochemical analyzer (Ivium Technologies) at a scan rate of 0.5 mV s^{-1}. Electrochemical impedance spectroscopy (EIS) was performed on the cells over the frequency range of 100 kHz to 0.01 Hz using the same electrochemical workstation with an amplitude of AC signal of 5 mV.

Acknowledgements

This work is supported by School of Materials and Energy, Guangdong University of Technology, P.R. China and Australian Research Council (ARC) Discovery & Linkage projects. Deakin University's Advanced Characterization Facilities are also acknowledged. The authors thank Timcal Ltd. for providing a sample of Super P Li carbon black. All authors discussed the results and contributed equally.

Keywords: polyanionic compound · amorphous $KFePO_4$/C · electrochemically active · high reversibility · potassium-ion batteries

[1] Y. Marcus, *Pure Appl. Chem.* **1985**, *57*, 1129.
[2] N. Matsuura, K. Umemoto, Z. Takeuchi, *Bull. Chem. Soc. Jpn.* **1974**, *47*, 813.
[3] S. Komaba, T. Hasegawa, M. Dahbi, K. Kubota, *Electrochem. Commun.* **2015**, *60*, 172.
[4] A. Eftekhari, Z. Jian, X. Ji, *ACS Appl. Mater. Interfaces* **2017**, *9*, 4404.
[5] M. Dahbi, N. Yabuuchi, K. Kubota, K. Tokiwa, S. Komaba, *Phys. Chem. Chem. Phys.* **2014**,*16*,15007.
[6] N. Yabuuchi, K. Kubota, M. Dahbi, S. Komaba, *Chem. Rev.* **2014**, *114*,11636.
[7] H. Kim, H. Ji, J. Wang, G. Ceder, *Trends in Chemistry*, doi.org/10.1016/j.trechm.2019.04.007.
[8] I. Sultana, T. Ramireddy, M. M. Rahman, Y. Chen, A. M. Glushenkov, *Chem. Commun.* **2016**, *52*, 9279.
[9] I. Sultana, M. M. Rahman, J. Liu, N. Sharma, A. V. Ellis, Y. Chen, A. M. Glushenkov, *J. Power Sources* **2019**, *413*, 476.
[10] I. Sultana, M. M. Rahman, T. Ramireddy, Y. Chen, A. M. Glushenkov, *J. Mater. Chem. A* **2017**, *5*, 23506.
[11] I. Sultana, M. M. Rahman, Y. Chen, A. M. Glushenkov, *Adv. Funct. Mater.* **2017**, 1703857.
[12] V. Mathew, S. Kim, J. Kang, J. Gim, J. Song, J. P. Baboo, W. Park, D. Ahn, J. Han, L. Gu, Y. Wang, Y. S. Hu, Y. K. Sun, J. Kim, *NPG Asia Mater.* **2014**, *6*, e138.
[13] K. Kubota, M. Dahbi, T. Hosaka, S. Kumakura, S. Komaba, *Chem. Rec.* **2018**, *18*, 459.
[14] T. Hosaka, T. Shimamura, K. Kubota, S. Komaba, *Chem. Rec.* **2019**, *19*, 735.
[15] M. Tang, W. C. Carter, Y. M. Chiang, *Ann. Rev. Mater. Res.* **2010**, *40*, 501.
[16] C. M. Julien, *Mat. Sci. Eng. R* **2003**, *40*, 47.
[17] J. Kim, A. Manthiram, *Nature* **1997**, *390*, 265.
[18] P. P. Prosini, M. Lisi, S. Scaccia, M. Carewska, F. Cardellini, M. Pasquali, *J. Electrochem. Soc.* **2002**, *149*, A297.
[19] X. H. Ma, F. Zhang, Y. Y. Wei, J. H. Zhou, J. Wang, W. Jia, Z. F. Zi, J. M. Dai, *J. Alloys Compd.* **2018**, *768*, 181.
[20] Y. Zhao, K. Yao, Q. Cai, Z. J. Shi, M. Q. Sheng, H. Y. Lin, M. W. Shao, *CrystEngComm* **2014**, *16*, 270.
[21] S. B. Yang, G. L. Cui, S. P. Pang, Q. Cao, U. Kolb, X. L. Feng, J. Maier, K. Mullen, *ChemSusChem* **2010**, *3*, 236.
[22] D. W. Wang, F. Li, M. Liu, G. Q. Lu, H. M. Cheng, *Angew. Chem. Int. Ed.* **2008**, *47*, 373.
[23] S. M. Oh, S. T. Myung, J. Hassoun, B. Scrosati, Y. K. Sun, *Electrochem. Commun.* **2012**, *22*, 149.
[24] L. X. Yuan, Z. H. Wang, W. X. Zhang, X. L. Hu, J. T. Chen, Y. H. Huang, J. B. Goodenough, *Energy Environ. Sci.* **2011**, *4*, 269.
[25] C. Li, X. Miao, W. Chu, P. Wu, D. G. Tong, *J. Mater. Chem. A* **2015**, *3*, 8265.
[26] Y. Liu, N. Zhang, F. Wang, X. Liu, L. Jiao, L. Z. Fan, *Adv. Funct. Mater.* **2018**, *28*, 1801917.
[27] L. F. Jiao, H. T. Yuan, Y. C. Si, Y. J. Wang, Y. M. Wang, *Electrochem. Commun.* **2006**, *8*, 1041.
[28] Y. Shao, M. Engelhard, Y. Lin, *Electrochem. Commun.* **2009**, *11*, 2064.

Manuscript received: November 4, 2019
Revised manuscript received: January 2, 2020
Accepted manuscript online: January 10, 2020
Version of record online: January 23, 2020